The vibrational spectrum of the hydrated proton: Comparison of experiment, simulation, and normal mode analysis

Jeongho Kim[a)]
Department of Chemistry, The James Franck Institute and Institute for Biophysical Dynamics, University of Chicago, Chicago, Illinois 60637

Udo W. Schmitt[a)]
Department of Chemistry and Henry Eyring Center for Theoretical Chemistry, University of Utah, Salt Lake City, Utah 84112-0850

Julie A. Gruetzmacher
Department of Chemistry, The James Franck Institute and Institute for Biophysical Dynamics, University of Chicago, Chicago, Illinois 60637

Gregory A. Voth[b)]
Department of Chemistry and Henry Eyring Center for Theoretical Chemistry, University of Utah, Salt Lake City, Utah 84112-0850

Norbert E. Scherer[b)]
Department of Chemistry, The James Franck Institute and Institute for Biophysical Dynamics, University of Chicago, Chicago, Illinois 60637

(Received 4 June 2001; accepted 8 October 2001)

The vibrational properties of the hydrated proton and deuteron in bulk phase water and deuterated water are investigated spectroscopically and computationally. Mid-infrared spectra of aqueous acid solutions are measured by attenuated total reflectance-Fourier transform IR spectroscopy and compared with pure water and salt/counterion spectra to extract high-quality hydrated proton spectra at a series of concentrations. Multistate empirical valence bond simulations of the excess proton in bulk phase water are also performed, allowing the autocorrelation function of the time derivative of the dipole moment, and hence the power spectrum of the hydrated proton, to be evaluated. The experimental and theoretical spectra are found to be in very good agreement. Normal mode analysis of the bulk phase simulation data allows definitive assignment of the spectrum. The associated motions are found to be represented by both Eigen and Zundel forms of the hydrated proton. [DOI: 10.1063/1.1423327]

I. INTRODUCTION

Proton transport in aqueous media is one of the most important processes in chemistry and biology and has been the subject of intense experimental and theoretical scrutiny for many decades.[1–12] The hydrated proton shows anomalously high mobility in aqueous media compared to other electrolytic species,[5] indicating that transport occurs via mechanisms other than normal ionic diffusion. Some of the most interesting cases occur in biology where proton transport plays a key role in function, e.g., proton permeation along a one-dimensional water chain in ion channels.[7] Thus, a complete description of proton transport in liquid water is crucial for a molecular level understanding of a wide range of reactions and processes in aqueous environments. In particular, thorough characterization of the transport behavior of the excess proton in water is an important first step toward understanding proton transport in more complex environments.

The unique structure of water and significant quantum mechanical contributions to pure water dynamics[8,13] lead to other unique consequences. The commonly accepted mechanism of proton transport in liquid water is that the excess positive charge, not the proton itself, migrates through the hydrogen-bonded network by a concerted series of hydrogen-bond formation and breaking steps. This structural diffusion process is termed the Grotthus mechanism.[9] Even though there is general agreement on the basis of the structural diffusion mechanism, a detailed description of molecular motions limiting the migration rate of the excess proton in the process has only recently been proposed.[10]

The multistate empirical valence bond (MS-EVB) method for determining reactive ground state potential energy surfaces (PES) was developed by Schmitt and Voth[8,11] and applied to a comprehensive computational study of proton transport in water.[8,13,14] Quantum centroid molecular dynamics simulations of the excess proton in bulk water yielded a proton transport rate in good agreement with the experimental value. The MS-EVB methodology has also allowed critical analysis of the ''Moses mechanism'' of proton transport in water, first proposed by Agmon,[12] which in-

[a)]Contributed equally to this work.
[b)]Authors to whom correspondence should be addressed. Electronic mail: voth@chemistry.utah.edu, nfschere@uchicago.edu

volves hydrogen-bond breaking in the second solvation shell of the hydronium ion as the rate-limiting step in proton transport. The finding of this analysis is that the critical H-bond-breaking step is likely to occur for a water molecule in the first solvation shell of the hydronium ion (or, equivalently, for a water in the first solvation shell of the Eigen cation). This mechanism is a modification of the one proposed by Agmon. Therefore, the MS-EVB approach is a powerful computational approach for the investigation of proton transfer dynamics.

An experimental approach to study the microscopic environments of relevance to proton transfer is vibrational spectroscopy. Infrared absorption spectroscopy is a valuable tool for probing molecular environments as the frequency (i.e., energy) and profiles (shapes and widths) of vibrational transitions are strongly influenced by interactions with their surroundings.[15] Infrared spectroscopy is especially valuable for studying hydrogen-bonded systems as the peak positions and widths of transitions involving hydrogen-bonded groups are highly sensitive to the extent of hydrogen bonding.[16] Many investigations into the hydrogen-bonding structure of aqueous systems have involved measurement and analysis of their infrared spectra.[17–24] While powerful, this approach is limited in a number of significant ways. First, traditional transmission spectroscopy is difficult to accomplish reliably in practice due to the high sample absorptivity resulting from the high number density of OH oscillators. Second, the broad absorption band characteristic of such systems washes out details of the dynamic processes contributing to the line shapes, making the assignment of molecular motions to the absorption bands difficult. This is particularly true in the case of the excess proton in water: Although there have been numerous studies to measure the IR spectrum of hydrated protons in aqueous solutions, the spectra and the assignment of the absorption bands have been inconsistent.[25–28] Furthermore, the identity of the primary hydrated proton ''species'' in liquid water and the transient structures involved in the proton transfer process have been controversial issues.[6,29,30] The utility of vibrational spectroscopy for characterizing the hydrated proton hinges on the measurement of reliable infrared spectra and a firm basis for assigning the molecular motions contributing to the absorption bands. In theoretical studies by Tuckerman *et al.*[31–33] on the properties of an excess proton in bulk phase water as well as in the MS-EVB studies,[8,10] it was proposed that proton transfer occurs by the interplay of two distinct species, the Zundel cation ($H_5O_2^+$) and the Eigen cation ($H_9O_4^+$). A normal mode analysis of these two complexes is essential to assign the absorption bands.

This paper is a joint experimental and theoretical effort aimed at understanding proton transport by way of comparing the results of a computer simulation model of the hydrated proton with an accurate vibrational spectrum thereof. Mid-IR spectra (500–4000 cm^{-1}) of acid, water and electrolyte solutions were measured, and appropriate difference spectra were constructed to extract the hydrated proton spectrum. Molecular dynamics (MD) simulations of the excess proton in water were performed with the MS-EVB approach. Vibrational spectra were derived from the dipole derivatives, and the partitioning of the Zundel ($H_5O_2^+$) and Eigen ($H_9O_4^+$) cation forms was determined via density of states calculations. A complete and reliable assignment of experimental spectral features is achieved through normal mode analysis for both the Zundel and Eigen cations, which have been reported to be the two main species involved in the proton migration through the hydrogen bonds.[31–33]

The organization of this paper is as follows: The experimental details are described in Sec. II, while the simulation approach is described in Sec. III. The experimental and simulation results are presented and discussed in Sec. IV, including the peak assignments by normal mode analysis. The results are summarized in Sec. V.

II. EXPERIMENT

A. Methods

Infrared transmission measurements[34] of hydrated protons are of limited value due to a typically low signal-to-noise ratio resulting from the sample's very large absorption coefficients. This complication is circumvented by the attenuated total reflection (ATR) technique. The evanescent wave-sample interaction in ATR-FTIR spectroscopy establishes a very thin effective path length appropriate for obtaining sufficiently good signal-to-noise ratio and highly reproducible spectra for spectral differencing. Thereby, the weak spectral contributions of dilute species can be isolated from the strong background. This method has been used to acquire IR spectra of liquid H_2O, D_2O, and isotopically diluted water samples,[19–21] and to determine the optical constants of water over a $\sim$15 000 cm^{-1} range.[22]

IR spectra were measured with a Bio-Rad FTS6000 FTIR spectrometer equipped with a liquid nitrogen-cooled MCT detector and an ATR accessory (Pike). The ZnSe crystal ATR accessory was positioned in a dry-nitrogen purged and temperature stabilized sample compartment facilitating long term and reproducible measurements. The trough with a ZnSe crystal bottom was filled with 2 ml of sample solution, and the spectra were taken with 2 cm^{-1} resolution; 128 scans were averaged for each spectrum shown. The raw spectral data were ratioed to the spectrum of the bare crystal on an absorbance scale. The final spectrum was obtained with ATR spectral correction to compensate for the higher absorption in the longer wavelength region, which is caused by the wavelength-proportional penetration depth of the evanescent wave into the sample.[35]

B. Sample

Infrared spectra of aqueous solutions of hydrochloric acid (HCl, Fisher Scientific, 37.4% solution) and hydrobromic acid (HBr, Fisher Scientific, 48% solution) were measured at a series of concentrations: 0.25, 0.5, 1.0, and 1.5 M. The effect of the counterion on the acid spectra was established by measurements of sodium chloride (NaCl, Acros, crystals, 99+%) and potassium chloride (KCl, Acros, crystals) aqueous solutions at the corresponding concentrations. All the aqueous solutions were prepared in deionized water (18.2 MΩ). In order to explore the effects of deuteration, IR

spectra of deuterium chloride (DCl, Janssen Chimica, 99+% D) in D_2O (Acros, 99.8% D) were measured at the same concentrations. To prevent contamination by water vapor, the solutions were prepared by adding DCl directly to the D_2O in the ATR crystal trough upon opening the bottle and spectra were immediately recorded. IR spectra of NaCl solutions in D_2O were also taken to consider the counterion effect. To emphasize the difference between the acid solution and pure water spectra, the IR spectrum of pure water (or D_2O for the deuteron case) was measured and subtracted from the solution spectra described above.

III. THEORY

The IR absorption spectrum of the hydrated excess proton in liquid water at room temperature can be computed from the Fourier transform of the dipole autocorrelation function:

$$I(\omega)=\frac{\hbar\beta}{2\pi}\omega^2\int dt e^{-i\omega t}\langle \boldsymbol{\mu}(0)\boldsymbol{\mu}(t)\rangle. \tag{1}$$

For computational and interpretative purposes, it is, however, more convenient to compute the autocorrelation function of the time derivative of the dipole moment:

$$I(\omega)=\frac{\hbar\beta}{2\pi}\int dt e^{-i\omega t}\langle \dot{\boldsymbol{\mu}}(0)\dot{\boldsymbol{\mu}}(t)\rangle. \tag{2}$$

The time derivative of the dipole moment within the point charge approximation assumed in the multistate empirical valence bond (MS-EVB) approach[8,11] is given by

$$\dot{\mu}(t)=\sum_{i}^{N_{\text{atom}}}[\dot{q}_i(t)\mathbf{R}_i(t)+q_i(t)\dot{\mathbf{R}}_i(t)]. \tag{3}$$

The first term in the sum can be regarded as the change in the dipole moment due to the adiabatic following of the electronic degrees of freedom (and therefore the point charges q_i) in time, whereas the second term is dominated by the time variation of the nuclear degrees of freedom, e.g., the velocities. The charges, q_i, are calculated via

$$q_i=\sum_{k}^{N_{EVB}} c_k^2 q_k^i, \tag{4}$$

with q_k^i being the partial charge on atom i in the kth VB state and c_k^2 being the corresponding EVB amplitude.

A classical MD simulation in the microcanonical (NVE) ensemble with 125 water molecules and one excess proton with an average kinetic temperature of 300 K was performed. The details are described elsewhere.[8] Two different dipole autocorrelation functions were calculated. First, the time derivative of the dipole moment of a cluster in the bulk consisting of six water molecules and the excess proton was evaluated; the selected water molecules were those with the highest EVB amplitudes (therefore being in spatial proximity to the excess proton). Second, the pure liquid water time derivative dipole autocorrelation function has been computed using six (selected) water molecules that are not directly electronically coupled to the excess charge. The same methodology was also used in the fully deuterated simulations where all the hydrogen nuclei of the system were replaced by deuterons. It should be noted that the ''cluster'' is actually a snapshot taken from the liquid configuration and therefore reflects the liquid state proportions of the Eigen to Zundel cation. An enlargement of this cluster to include 12 water molecules did not affect the results above 1000 cm^{-1}.

In order to help assign the different peaks in the IR spectrum to distinct vibrational modes of the excess proton, an instantaneous normal mode (INM) analysis[36,37] was performed. To do so, the $H^+/6H_2O$ cluster described in the previous paragraph was extracted from the bulk phase simulation every 5 fs, where the water molecules were the ones in spatial proximity to the excess proton. For every cluster snapshot from the liquid, the Hessian matrix was calculated, diagonalized, and the frequencies and corresponding instantaneous normal modes extracted. Imaginary frequencies, which are mainly localized in the 0 to 800 cm^{-1} frequency interval, were disregarded in the analysis process. A total of 20 000 cluster configurations were used for spectral evaluation.

IV. RESULTS AND DISCUSSION

A. Experimental results

1. Acid and electrolyte solutions

IR spectra of 1.0 M HCl and HBr solutions and pure water are shown in Fig. 1(a) (spectra of the solutions at other concentrations are not shown). In the pure water spectrum as well as in the spectra of the acid solutions, three broadbands are observed at 760, 1635, and 3350 cm^{-1}, which are assigned to libration, bending, and stretching motions of pure water molecules, respectively.[25] A small broad peak is also observed at 2100 cm^{-1}, which arises from the combination of libration and bending motions of water. Besides these absorption bands of pure water, additional features contribute to the spectra of both HCl and HBr solutions. A continuous absorption is observed over the broad range from 1000 to 3400 cm^{-1}, and a small peak is found at 1200 cm^{-1}. The spectra of the HCl and HBr solutions are nearly identical; it is difficult to distinguish between them, suggesting that the halogen counterions only make small contributions to the spectra.

The continuous absorption shown in Fig. 1(a) is regarded as a ubiquitous property of hydrogen-bonded systems.[25,26,28–30] It was first observed in the spectra of HCl and NaOH,[26] and it is believed to be caused by the presence of strong hydrogen bonds in a strongly solvating medium, such as those associated with the $H_5O_2^+$ and $H_3O_2^-$ ions in aqueous solution.[38,39] In general, it is considered to arise from the strong coupling of the proton transitions with collective vibrational excitations in the surrounding hydrogen-bonded solvating water molecules.

To clarify the spectral features of the hydrated proton, the pure water spectrum was subtracted from the acid solution spectra. The resulting difference spectra for 1.0 M HCl and HBr solutions are shown in Fig. 1(b). The three broadbands at 1760, 2900, and 3350 cm^{-1} as well as the broad peak at 1200 cm^{-1} and the continuous absorption over the 1000 to 3400 cm^{-1} range are the dominant features. All of

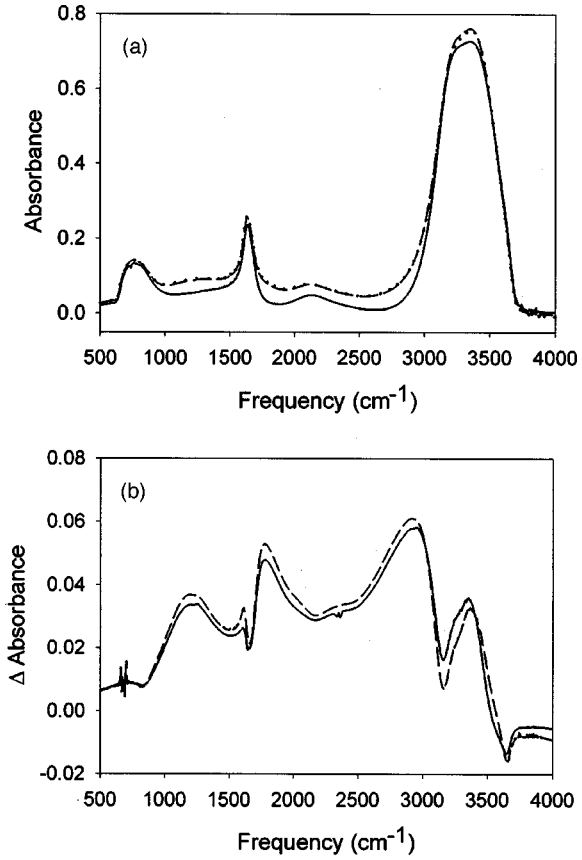

FIG. 1. (a) Infrared spectra of pure water and 1.0 M aqueous solutions of hydrochloric acid (HCl) and hydrobromic acid (HBr): water, solid; 1.0 M HCl, dashed; 1.0 M HBr, dotted. (b) Difference spectra of 1.0 M aqueous solutions of acid (HCl and HBr) and pure water: 1.0 M HCl–water, solid; 1.0 M HBr–water, dashed.

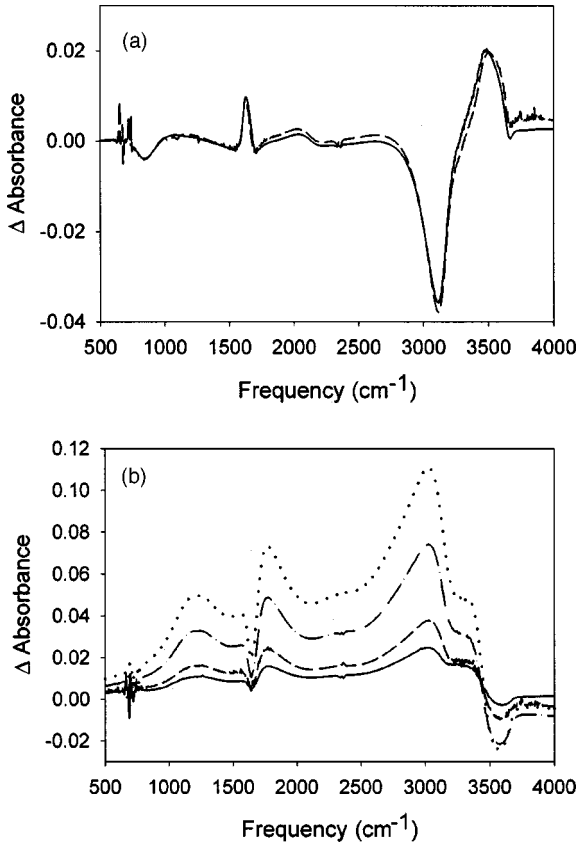

FIG. 2. (a) Difference spectra of 1.0 M electrolyte (NaCl and KCl) solutions and pure water: 1.0 M NaCl–water, solid; 1.0 M KCl–water, dashed. (b) Difference spectra of HCl aqueous solutions at various concentrations and NaCl solutions of the corresponding concentrations: 0.25 M HCl–0.25 M NaCl, solid; 0.5 M HCl–0.5 M NaCl, dashed; 1.0 M HCl–1.0 M NaCl, dashed-dotted; 1.5 M HCl–1.5 M NaCl, dotted.

these features can be attributed to the hydrated protons. The fact that both HCl and HBr solutions give almost identical difference spectra suggests a weak influence of the anionic counterion.

The frequencies of the absorption bands attributed to the hydrated protons in the present measurement are in good agreement with other studies.[25–28,40] Falk and Giguere,[25] who measured the infrared transmission spectra of aqueous solutions of mineral acids, observed concentration-dependent absorption bands in three frequency regions, 1205, 1750, and 2900 cm^{-1}, with continuous absorption ranging from 1000 to 3500 cm^{-1} in the HCl solution/water difference spectrum. In their assignment of the absorption bands, based on the existence of the hydronium ion (H_3O^+), the first two bands were assigned as ν_2 symmetric bending and ν_4 asymmetric bending, respectively, while the other was assigned as $\nu_3+\nu_1$ stretching of the hydronium ion. Librovich *et al.*[28] also reported absorption bands attributed to hydrated protons at 1170 cm^{-1} (asymmetric stretching of OHO fragment in $H_5O_2^+$), 1710 cm^{-1} (bending of OH_2 group in $H_5O_2^+$) and 2900 cm^{-1} (stretching of OH_2 group in $H_5O_2^+$) with continuous absorption at 1000–3400 cm^{-1}; the peak positions agree well with the results of Falk and Giguere. However, they assigned the peaks based on the existence of $H_5O_2^+$, the so-called Zundel cation, instead of the hydronium ion.

The IR spectra of aqueous NaCl and KCl solutions were measured to investigate the manifestation of the counterion therein. The difference spectra of 1.0 M NaCl and KCl (solutions minus pure water) are shown in Fig. 2(a). Compared to the acid solutions, the ionic solution difference spectra exhibit only small changes in absorbance. Furthermore, the NaCl and KCl difference spectra are virtually identical, suggesting that the cations either make negligible or identical contributions. Two small positive peaks at 1625 and 3500 cm^{-1} and a relatively larger negative feature at 3120 cm^{-1} are observed. Considering its amplitude, the negative feature accounts for the large dip in the acid solution difference spectra at 3150 cm^{-1}. Minor contributions to the other peaks are also observed. To eliminate the effect of the anionic counterion, the NaCl solution spectrum, instead of the pure water one, was subtracted from the HCl solution spectrum at the same concentrations. The resulting spectra for various concentrations are shown in Fig. 2(b). The resulting spectra become more "rounded," especially between the 2900 and 3350 cm^{-1} bands, resulting in a merging of the two bands. The absorption at the main bands (1250, 1760, 3020 cm^{-1}) and the continuum absorption (e.g., at 1500, 2200, and 2500 cm^{-1}) exhibit a highly linear dependence on concentration, i.e., Beer's law behavior. Therefore, the resulting difference spectrum obtained by subtracting the electrolyte spectrum is regarded as the vibrational spectrum of hydrated proton.

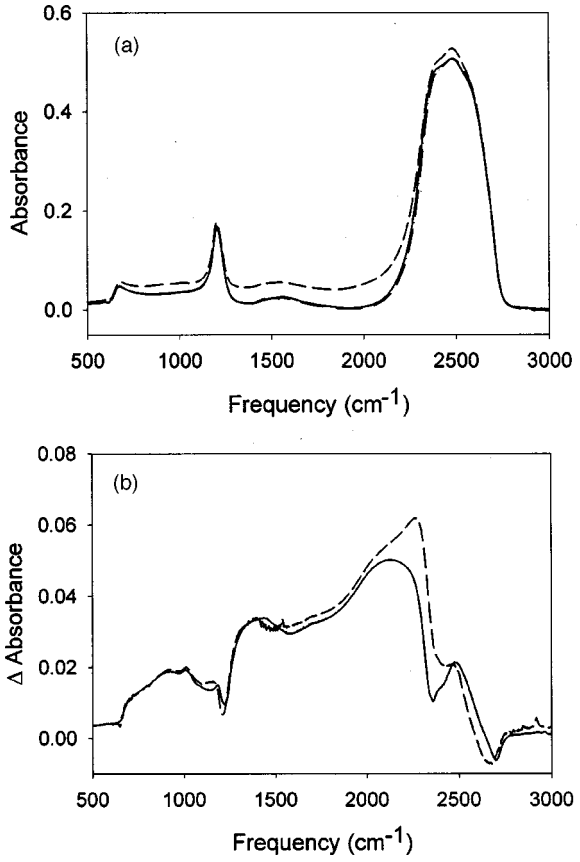

FIG. 3. (a) Infrared spectra of pure heavy water (D_2O) and 1.0 M deuterium chloride (DCl) and sodium chloride (NaCl) solutions in heavy water: D_2O, solid; 1.0 M DCl/D_2O, dashed; 1.0 M NaCl/D_2O, dashed-dotted. (b) Difference spectrum of 1.0 M DCl/D_2O solution and pure D_2O (solid) and difference spectrum of 1.0 M DCl/D_2O solution and 1.0 M NaCl/D_2O solution (dashed).

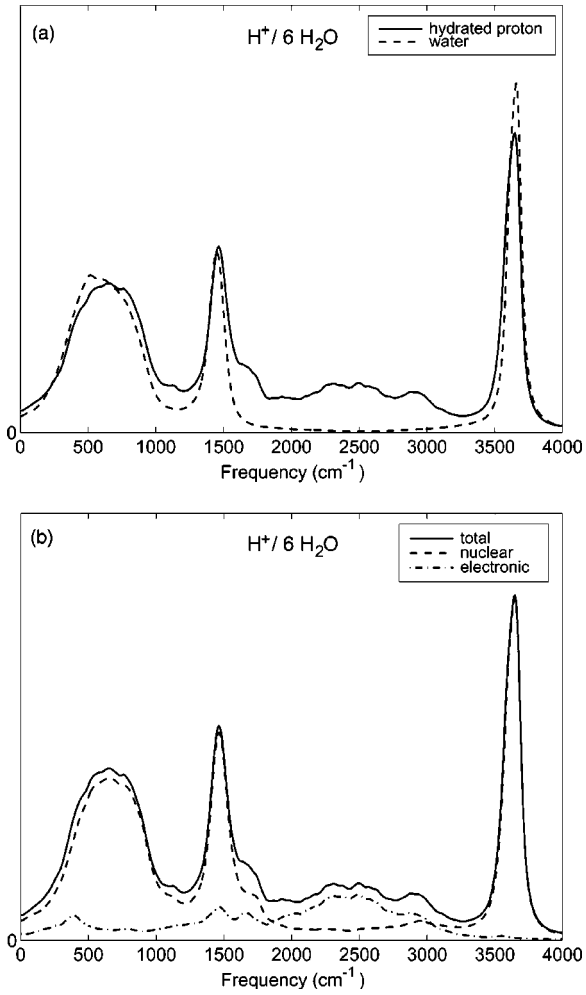

FIG. 4. (a) Power spectrum of the dipole time derivative autocorrelation function for the hydrated excess proton (solid) and pure water (dashed). (b) Power spectrum of the total (solid), nuclear (dashed) and electronic (dashed-dotted) contribution to the dipole time derivative autocorrelation function for the hydrated excess proton.

2. Deuterated acid solutions

IR spectra of D_2O and a 1.0 M DCl solution are shown in Fig. 3(a). Three broadbands are observed at 680, 1200 and 2480 cm^{-1} that, respectively, correspond to the transitions at 760, 1635, and 3350 cm^{-1} in H_2O; these can be assigned to libration, bending and stretching motions of D_2O. In addition to the D_2O bands, the DCl solution spectrum also shows a continuous absorption in the 1300–2250 cm^{-1} region. A small band centered at 920 cm^{-1} also appears that corresponds to the 1200 cm^{-1} peak in the HCl/H_2O spectrum.

These features become more apparent in the difference spectra (solution minus D_2O) shown in Fig. 3(b). Again, each peak in the deuterated difference spectrum has its counterpart in the proton difference spectrum with red-shifted frequencies. The general shape of the spectrum also agrees well with that for HCl, but over a compressed spectral range as expected from the greater mass of the deuteron. The continuous absorption in the 1300–2250 cm^{-1} region is more evident. Furthermore, the absorbance of all the bands, including that at 920 cm^{-1}, increase linearly in magnitude with DCl concentration. Besides these features, four more peaks are observed near 1420, 2130, 2480, and 3415 cm^{-1}. The first three peaks correspond to the peaks at 1760, 2900, and 3350 cm^{-1} in the HCl/H_2O spectrum. The small peak at 3415 cm^{-1} seems to arise from contamination by H_2O absorption from the air; it increased as the measurement (i.e., exposure) time increased (spectra not shown). The NaCl in D_2O solution spectrum was subtracted from the DCl spectrum to eliminate the counterion effect. This resulted in the merging of the 2130 and 2480 cm^{-1} peaks as seen as the dashed curve in Fig. 3(b) superimposed on the DCl/D_2O difference spectrum. This is the same change as observed in the HCl/NaCl difference spectrum.

B. Simulation results

The simulated IR spectra corresponding to the protonated cluster and the pure water cluster of the same size are shown in Fig. 4(a). In the pure water case, the well-known features of the spectrum (OH stretch: ~3600 cm^{-1}, HOH bend: ~1500 cm^{-1}, libration: ~600 cm^{-1}) are found as in the experimental spectrum [Fig. 1(a)]. For the protonated case, a gain in intensity over the broad range from 1550 to 3450 cm^{-1} is observed, i.e., the so-called continuum band, whereas the intensity of the peak corresponding to the OH stretch is reduced somewhat. In order to shed light on the

origin of the continuum band, the time derivative of the dipole moment, Eq. (2), was decomposed into two terms, which can be regarded as electronic and nuclear components:

$$\dot{\boldsymbol{\mu}}(t)=\dot{\boldsymbol{\mu}}_{el}(t)+\dot{\boldsymbol{\mu}}_{nu}(t)$$
$$=\sum_{i}^{N_{\text{atom}}}\dot{q}_i(t)\mathbf{R}_i(t)+\sum_{i}^{N_{\text{atom}}}q_i(t)\dot{\mathbf{R}}_i(t). \tag{5}$$

The change of $\dot{\boldsymbol{\mu}}_{el}(t)$ is dominated by the time derivation of the point charges, $\dot{q}_i$, caused by the adiabatic following of the electronic degrees of freedom on displacement of the nuclei, whereas $\dot{\boldsymbol{\mu}}_{nu}(t)$ is dominated by the nuclear velocity, $\dot{\mathbf{R}}_i(t)$, such that

$$\langle\dot{\boldsymbol{\mu}}(0)\dot{\boldsymbol{\mu}}(t)\rangle=\langle\dot{\boldsymbol{\mu}}(0)_{el}\dot{\boldsymbol{\mu}}(t)_{el}+\dot{\boldsymbol{\mu}}(0)_{nu}\dot{\boldsymbol{\mu}}(t)_{nu}$$
$$+\dot{\boldsymbol{\mu}}(0)_{nu}\dot{\boldsymbol{\mu}}(t)_{el}+\dot{\boldsymbol{\mu}}(0)_{el}\dot{\boldsymbol{\mu}}(t)_{nu}\rangle$$
$$\approx\langle\dot{\boldsymbol{\mu}}(0)_{el}\dot{\boldsymbol{\mu}}(t)_{el}\rangle+\langle\dot{\boldsymbol{\mu}}(0)_{nu}\dot{\boldsymbol{\mu}}(t)_{nu}\rangle. \tag{6}$$

Note that the separation between nuclear and electronic contributions does not strictly apply, so both terms will have (small) contributions from the complementary set of degrees of freedom. For comparison, both the electronic term $\langle\dot{\boldsymbol{\mu}}(0)_{el}\dot{\boldsymbol{\mu}}(t)_{el}\rangle$ and the nuclear term $\langle\dot{\boldsymbol{\mu}}(0)_{nu}\dot{\boldsymbol{\mu}}(t)_{nu}\rangle$ were computed and Fourier transformed independently. The corresponding spectra, together with the total calculated IR spectra from Fig. 4(a), given by the exact result in Eq. (6), are shown in Fig. 4(b). It can be seen that the nuclear contribution is clearly the dominant part of the IR spectrum, especially in the frequency ranges that can be connected to pure water vibrations. However, the electronic contribution adds significant intensity to the spectrum in the 1600–3400 cm^{-1} range. This shows that approximating the IR spectrum by including only the nuclear dephasing (e.g., using the velocity autocorrelation function) will most likely fail to give the correct IR spectral intensities.

In order to make a connection to the experimental results in this paper, the two spectra shown in Fig. 4(a) were subtracted; the result is shown together with the experimental result in Fig. 5. The experimental difference spectra (lower panel) show a negative peak at 3650 cm^{-1}, two broad positive peaks at 3300 and 3000 cm^{-1}, a broad positive continuum ranging from 3400 to 1000 cm^{-1} with a peak at 1760 cm^{-1}, immediately followed by a dip at 1650 cm^{-1}. All of these features of the experimental spectrum can be seen in the theoretical calculation (upper panel), with peak locations being slightly red- or blue-shifted and intensities in overall good agreement with the experiment.

The computed difference spectrum for deuterated case where all the protons are replaced by deuterons is also shown with the experimental difference spectrum of DCl in heavy water in Fig. 6. As in the protonated case, there is agreement of the features between the two spectra with good matching of peak positions.

C. Normal mode analysis and spectral interpretation

In order to attribute the peaks found in the difference spectrum to particular vibrational modes of the hydrated excess proton cluster, an instantaneous normal mode (INM) analysis[36,37] was performed. To do so, 20 000 different cluster configurations consisting of the excess proton and the six closest water molecules were cut out of the bulk phase simulation and the INM density of states, given by

$$\rho(\omega)=\left\langle\sum_{i=1}^{6N-M}\delta(\omega-\omega_i)\right\rangle \tag{7}$$

was computed. Here, N is the number of atoms in the cluster, and M accounts for the imaginary frequencies, which have been omitted in the analysis. The function $\rho(\omega)$ is compared

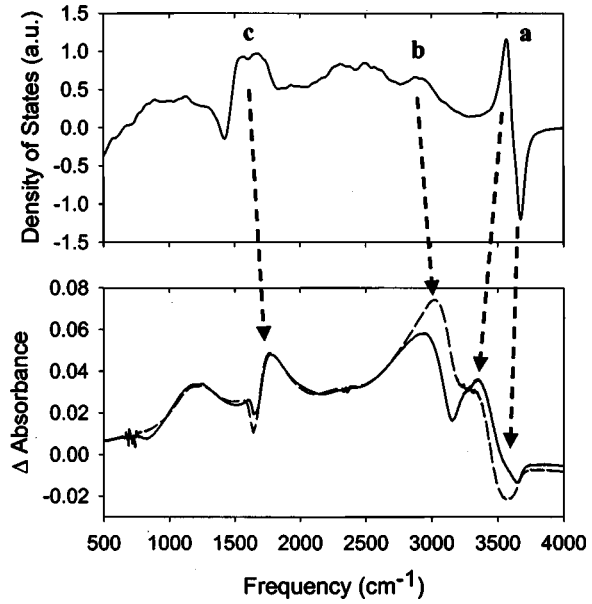

FIG. 5. Comparison of the computed IR difference spectrum (upper panel) with the experimental result (lower panel; 1.0 M HCl–water, solid; 1.0 M HCl–1.0 M NaCl, dashed). The dashed arrows indicate the corresponding peaks.

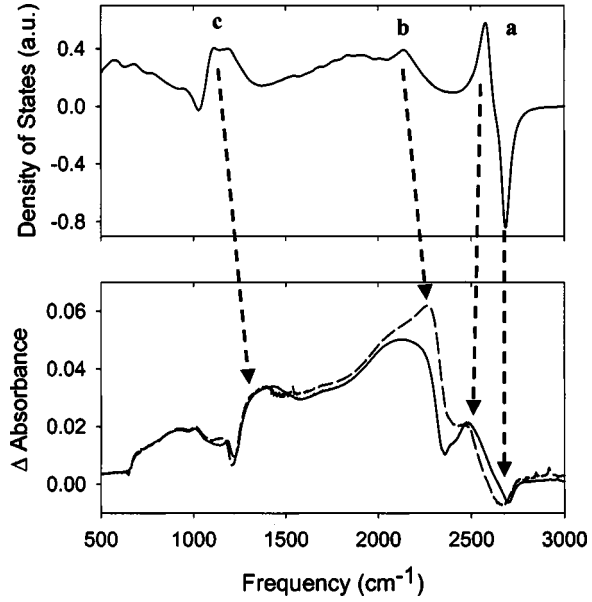

FIG. 6. Comparison of the computed IR difference spectrum (upper panel) with the experimental result (lower panel; 1.0 M DCl–D_2O, solid; 1.0 M DCl–1.0 M NaCl/D_2O, dashed) for deuterated case. The dashed arrows indicate the corresponding peaks.

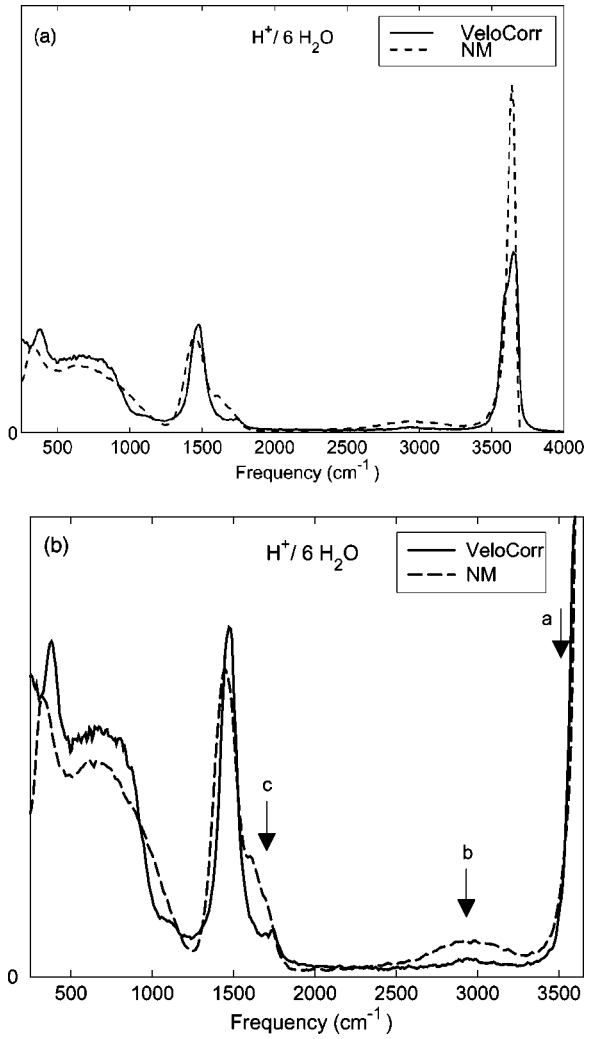

FIG. 7. Comparison of vibrational density of states obtained from the INM analysis (dashed) with the power spectrum of the velocity autocorrelation function (solid): (a) Frequency range 200–4000 cm^{-1}; (b) 200–3600 cm^{-1}.

to the density of states obtained from the Fourier transform of the velocity autocorrelation function, e.g., the second term in Eq. (6) with charges set to unity. Both densities are illustrated in Fig. 7(a); the peak positions of the two densities agree very well, but the peak intensities for the high frequency OH stretch densities differ by a factor of 2. Some of this difference can be attributed to anharmonic broadening of the velocity correlation function (i.e., MD) results. The two densities in the more relevant frequency range from 200 to 3600 cm^{-1} are shown in Fig. 7(b). The three arrows indicate the frequency ranges that will be examined in order to interpret the difference spectra in Fig. 5.

To this end, it is helpful to compute the INM density independently using the degree of hydrogen bond asymmetry of the shortest oxygen–oxygen bond in the protonated complex as a descriptor.[8] To do so for this bond, the asymmetric stretch coordinate

$$q = \frac{R_{OO}}{2} - R_{OH} \tag{8}$$

was computed and the averages in Eq. (7) were performed with the restriction $|q|<0.1$ (Zundel-like case) and $|q|>0.1$ (Eigen-like case), respectively. Both normalized densities are shown in Fig. 8. Note that the two densities will not add up to the total density shown in Fig. 7(a) due to the independent normalization performed.

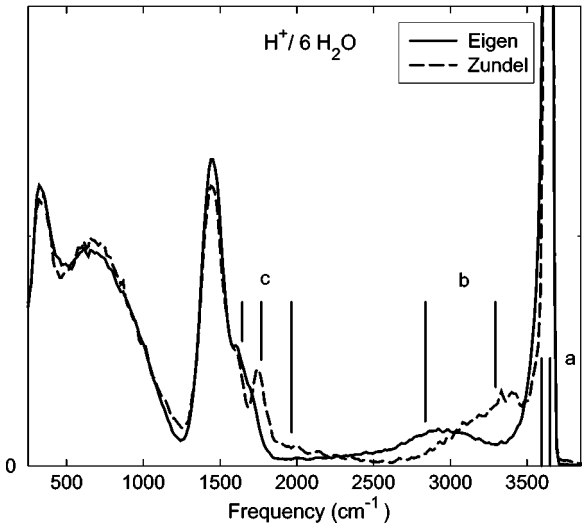

FIG. 8. Normalized INM density for $|q|>0.1$ (Eigen case; solid) and $|q|<0.1$ (Zundel case; dashed). The vertical lines show the regions that have been examined more closely in terms of their corresponding normal mode eigen vectors.

It is evident from Fig. 8 that the frequency regions indicated by a, b, and c in Fig. 7(b) gain different contributions from the Zundel-like or Eigen-like nuclear configurations. For the frequency ranges marked by the vertical lines in Fig. 8, the corresponding normal mode eigenvectors were stored independently and visualized afterwards. The results of that visualization analysis are displayed as the dominant local modes (stretching and bending motion) that contribute most to the normal mode. Note that the different normal modes within the given frequency ranges are regarded in the following as linear combinations of these local modes with varying amplitudes and phase factors.

Figure 9(a) displays the bending modes on the water oxygen with the largest hydronium character and the nearest neighbor water molecule that are responsible for the peaks at 1580–1640 cm^{-1} in the Eigen-like situation and 1680–1880 cm^{-1} in the Zundel case. Therefore, the contribution to the continuum band in that frequency range (''c'' in Fig. 5) stems from the bending motion in the hydronium ion or in the Zundel dimer, which are both blue-shifted compared to pure water. This explains the peak structure in region ''c'' in Fig. 5. The dip at the water bend frequency is due to the almost complete cancellation of the densities in the difference spectrum, whereas the peak at slightly larger wave numbers originates from the aforementioned bending motion of water molecules in close proximity to the excess proton.

Region ''b'' in Fig. 5 at 2700–2950 cm^{-1} corresponds to normal modes that are a linear combination of OH stretch vibrational motions in the symmetrically hydrated hydronium ion [Fig. 9(b)]. This is confirmed in Fig. 8, where the total INM density in that range is dominated by contributions from Eigen-like nuclear configurations with asymmetric hy-

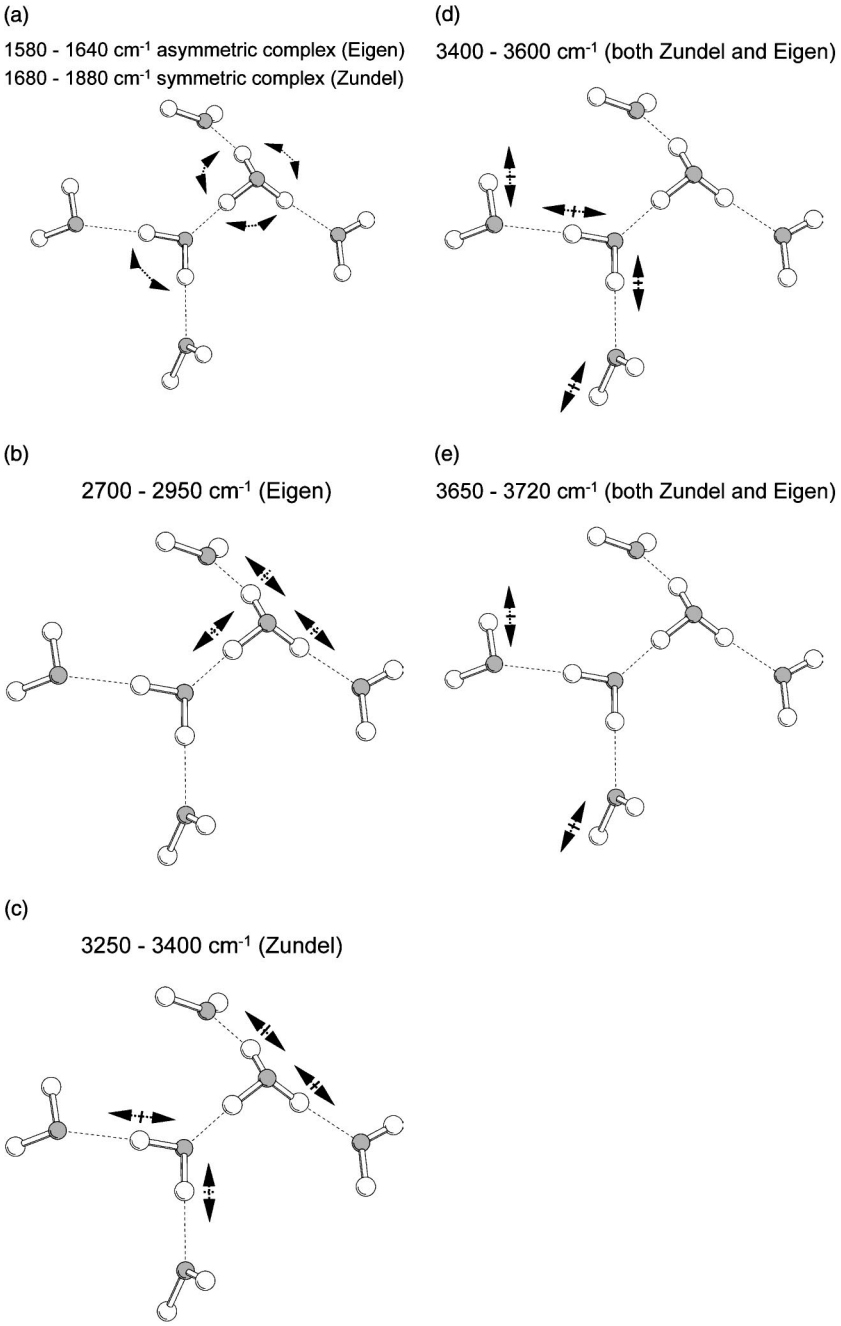

FIG. 9. Illustration of the relevant local modes participating in the normal modes in a given frequency interval for the protonated cluster $H^+ \cdot 6H_2O$. The same basic structure is used for all modes for compactness of presentation. In figures showing both Eigen and Zundel modes, it should be understood that the Zundel structure is symmetric with respect to the excess proton. (a) 1580–1880 cm^{-1}, bending modes on the center oxygen of the hydronium ion and the nearest neighbor water molecule; (b) 2700–2950 cm^{-1}, a linear combination of OH stretch motions in the symmetrically hydrated hydronium ion; (c) 3250–3400 cm^{-1}, a linear combination of OH stretch motions of the two water molecules which symmetrically solvate the excess proton; (d) 3400–3600 cm^{-1}, delocalized normal modes with OH stretch motions of water molecules in the first and second solvation shells of the hydronium ion; (e) 3650–3720 cm^{-1}, bulk water symmetric and asymmetric OH stretch motions.

drogen bonds. The peak in region ''b'' in Fig. 5 gains its intensity mainly from these stretching modes.

Moving to larger frequencies in the 3250–3400 cm^{-1} range, the main contribution to the density is shifted from the Eigen situation to the Zundel-like configuration. The corresponding normal modes in Fig. 9(c) can be regarded as a linear combination of OH stretch motions of the two water molecules which symmetrically solvate the excess proton (which itself is not moving).

The absorptions in the 3400–3600 cm^{-1} frequency range are constituted from fairly delocalized normal modes with OH stretch motions of water molecules in the first and second solvation shells of the H_3O^+ ion, with contributions from both Zundel and Eigen nuclear configurations [Fig. 9(d)]. The motions associated with the 3650 to 3720 cm^{-1} region are shown in Fig. 9(e); they correspond to the bulk water symmetric and asymmetric OH stretch motions.

This information can be used to explain the peak structure ''a'' in Fig. 5. The positive peak at ca. 3600 cm^{-1} in the computed spectrum originates from OH stretch motions of water molecules in the first and second solvation shells of the hydrated proton that are strongly coupled to the excess proton. The red-shift from pure water can be explained by the transfer of electron density from the hydrated water molecules to the hydronium ion, therefore weakening the water OH bond and dipole moment. The negative peak at ca. 3700 cm^{-1} in region ''a'' in Fig. 5 corresponds to those OH stretch vibrations of water that, on insertion of the excess proton, electronically couple to it and thus create the missing intensity in the difference spectrum. In other words, the OH

stretches of the water molecules in the first and second solvation shell around the hydronium ion, which show up slightly red-shifted, are not adding intensity in the 3700 cm^{-1} region in the hydrated proton spectrum, thus leading to the negative peak in the difference spectrum.

Upon comparison of the results from experiment and simulation (Fig. 5), there are, however, small discrepancies in the frequencies of the absorption bands. In particular, the simulated bands at lower frequencies, i.e., bending modes under 3000 cm^{-1}, are red-shifted relative to experiment and those in higher frequencies over 3000 cm^{-1}, i.e., stretching modes, are generally blue-shifted. There are several factors to consider. An anion exists in the experimental solutions with equal concentration to the proton, but counterions were not included in the simulations. It has been reported that the anion tends to deform the hydrated proton as well as water molecules.[25] The frequencies of the stretching modes in the experimental spectra would then be red-shifted by the existence of the anion through a weakening of the OH bonds in the hydrated proton. For similar reasons, the frequencies of the bending modes could be blue-shifted. In the high frequency OH stretching regions, the influence of quantization effects (not included in the simulations) can lead to red-shifts.[41] A more likely possibility for the deviation in frequencies, of course, are inaccuracies in the MS-EVB potential energy surface (e.g., from a primarily harmonic intramolecular potential) beyond neglecting the anion. A polarizable potential may also be important for making more quantitative comparisons with experiment since polarizability may have an influence on these motions.[42] Finally, quantum effects and delocalization character of the hydrogen atoms and the excess proton would tend to soften the high frequency ''local'' motions.[43]

V. SUMMARY AND CONCLUSIONS

This study investigated the behavior of hydrated protons in bulk phase water both spectroscopically and computationally. IR difference spectra of aqueous, acid and electrolyte solutions, obtained by ATR-FTIR spectroscopy with excellent signal-to-noise ratio, are reported. IR difference spectra (aqueous acid solutions minus pure water) show distinct spectral features of hydrated protons. The assignment of the absorption bands is made with the computed density of states associated with the hydrated proton (and analogous computational differencing). The resultant spectrum is in good agreement with experiment. The general shape of the difference spectra matches very well for both the protonated and deuterated cases except for small but clearly apparent frequency shifts of the absorption bands. These discrepancies might arise from the difference between the experimental and simulation conditions, e.g., the existence of counterions, or from limitations in the computational approach, e.g., the neglect of quantum effects in the dynamics and/or inaccuracies in the MS-EVB or water potentials. Nevertheless, the obvious correspondence allows the peaks in the spectrum to be assigned with a normal mode analysis performed with a basis set of MS-EVB states for the Zundel and Eigen cations. Each normal mode is visualized as local modes that dominantly contribute to the normal mode, giving rise to a more detailed picture of the nuclear motions associated with the hydrated proton in liquid water than previously reported.

New insights into the relationship between the spectral features and the behavior of the proton in bulk phase water will be helpful in understanding the transport process in bulk phase water as well as in studying microscopic dynamics of biochemical systems where the proton transfer plays a crucial role, for example, in gramicidin, a model ion channel.[44–51] Furthermore, the normal mode analysis method used in this study could be applied to nonlinear optical measurements[52] designed to resolve the dynamics associated with the hydronium ion.

ACKNOWLEDGMENTS

G.A.V. acknowledges support from the NSF (CHE9712884), and N.F.S. from the NIH (GM57768) with partial support from the University of Chicago NSF-sponsored MRSEC (DMR9808595). J.A.G. thanks the NSF for a predoctoral fellowship.

[1] *Water: A Comprehensive Treatise*, Vols. 1–7, edited by F. Franks (1972–1985).
[2] D. Eisenberg and W. Kauzman, *The Structure and Properties of Water* (Oxford University Press, Oxford, 1969).
[3] L. Stryer, *Biochemistry*, 3rd ed. (W. H. Freeman, New York, 1988).
[4] A. Lehninger, D. Nelson, and M. Cox, *Principles of Biochemistry*, 2nd ed. (Worth, New York, 1993).
[5] M. Eigen and L. D. Maeyer, Proc. R. Soc. London **247**, 505 (1958).
[6] M. Eigen, Angew. Chem. **3**, 1 (1964).
[7] B. Hille, *Ionic Channels of Excitable Membranes* (Sinauer Associates, Sunderland, 1991).
[8] U. W. Schmitt and G. A. Voth, J. Chem. Phys. **111**, 9361 (1999).
[9] C. v. Grotthuss, Ann. Chim. (Paris) **LVII**, 54 (1806).
[10] T. J. F. Day, U. W. Schmitt, and G. A. Voth, J. Am. Chem. Soc. **122**, 12027 (2000).
[11] U. W. Schmitt and G. A. Voth, J. Phys. Chem. B **102**, 5547 (1998).
[12] N. Agmon, Chem. Phys. Lett. **244**, 456 (1995).
[13] U. W. Schmitt and G. A. Voth, Isr. J. Chem. **39**, 483 (1999).
[14] U. W. Schmitt and G. A. Voth, Chem. Phys. Lett. **329**, 36 (2000).
[15] W. G. Rothschild, *Dynamics of Molecular Liquids* (Wiley, New York, 1984).
[16] G. C. Pimentel and A. L. McClellan, *The Hydrogen Bond* (W. H. Freeman, San Francisco, 1960).
[17] M. Falk and T. A. Ford, Can. J. Chem. **44**, 1699 (1966).
[18] T. A. Ford and M. Falk, Can. J. Chem. **46**, 3579 (1968).
[19] Y. Marechal, J. Chem. Phys. **95**, 5565 (1991).
[20] Y. Marechal, J. Phys. Chem. **97**, 2846 (1993).
[21] Y. Marechal, J. Mol. Struct. **322**, 105 (1994).
[22] J. E. Bertie and Z. Lan, Appl. Spectrosc. **50**, 1047 (1996).
[23] A. S. Gilbert and N. Sheppard, J. Chem. Soc. D 337 (1971).
[24] A. S. Gilbert and N. Sheppard, J. Chem. Soc., Faraday Trans. 2 **69**, 1628 (1973).
[25] M. Falk and P. A. Giguere, Can. J. Chem. **35**, 1195 (1957).
[26] T. Ackermann, Z. Phys. Chem. (Munich) **27**, 253 (1961).
[27] P. Rhine, D. Williams, G. M. Hale, and M. R. Querry, J. Phys. Chem. **78**, 1405 (1974).
[28] N. B. Librovich, V. P. Sakun, and N. D. Sokolov, Chem. Phys. **39**, 351 (1979).
[29] G. Zundel, *Hydration and Intermolecular Interaction* (Academic, New York, 1969).
[30] P. Schuster, G. Zundel, and C. Sandorfy, *The Hydrogen Bond, Recent Developments in Theory and Experiments* (North-Holland, Amsterdam, 1976).
[31] M. Tuckerman, K. Laasonen, M. Sprik, and M. Parrinello, J. Phys. Chem. **99**, 5749 (1995).
[32] M. Tuckerman, K. Laasonen, M. Sprik, and M. Parrinello, J. Phys. Chem. **6**, 93 (1994).
[33] D. Marx, M. E. Tuckerman, J. Hutter, and M. Parrinello, Nature (London) **397**, 601 (1999).

[34] *Hydrogen Bonded Liquids*, Vol. 329, edited by J. C. Dore and J. Teixeira (Kluwer Academic, Dordrecht, 1991).
[35] P. R. Griffith and J. A. d. Haseth, *Fourier Transform Infrared Spectroscopy* (Wiley, New York, 1986).
[36] M. Buchner, B. M. Ladanyi, and R. M. Stratt, J. Chem. Phys. **97**, 8522 (1992).
[37] M. Cho, G. R. Fleming, S. Saito, I. Ohmine, and R. M. Stratt, J. Chem. Phys. **100**, 6672 (1994).
[38] G. Zundel and H. Metzger, Z. Phys. Chem. (Munich) **59**, 225 (1968).
[39] T. Ackermann, G. Zundel, and K. Zwernemann, Ber. Bunsenges. Phys. Chem. **73**, 446 (1969).
[40] H. Downing and D. Williams, J. Phys. Chem. **80**, 1640 (1976).
[41] J. Lobaugh and G. A. Voth, J. Chem. Phys. **104**, 2056 (1996).
[42] B. Berne, private communication.
[43] C. Cohen-Tannoudji, *Quantum Mechanics* (Wiley, New York, 1977).
[44] D. V. Greathouse, J. F. Hinton, K. S. Kim, and R. E. Koeppe II, Biochemistry **33**, 4291 (1994).
[45] S. Naydenova, A. G. Petrov, and J. Yarwood, Langmuir **11**, 3435 (1995).
[46] D. E. Sagnella and G. A. Voth, Biophys. J. **70**, 2043 (1996).
[47] F. Bartl, B. Brzezinski, B. Rozalski, and G. Zundel, J. Phys. Chem. B **102**, 5234 (1998).
[48] J. Ha, C. S. Henry, and I. Fritsch, Langmuir **14**, 5850 (1998).
[49] B. M. Burkhart, R. M. Gassman, D. A. Langs, W. A. Pangborn, and W. L. Duax, Biophys. J. **75**, 2135 (1998).
[50] W.-P. Ulrich and H. Vogel, Biophys. J. **76**, 1639 (1999).
[51] S.-W. Chiu, S. Subramaniam, and E. Jakobsson, Biophys. J. **76**, 1929 (1999).
[52] M. F. Kropman and H. J. Bakker, Science **291**, 2118 (2001).